IEEE Access
Multidisciplinary : Rapid Review : Open Access Journal

Received September 30, 2020, accepted October 9, 2020, date of publication October 15, 2020, date of current version October 30, 2020.

Digital Object Identifier 10.1109/ACCESS.2020.3031295

Kinematic Model of the Human Leg Using DH Parameters

MARIO LLEWELLYN STRYDOM [1,2], ARTUR BANACH [1,2], JONATHAN ROBERTS [1,2], (Senior Member, IEEE), ROSS CRAWFORD [1,2,3], AND ANJALI TUMKUR JAIPRAKASH [1,2]

[1]Queensland University of Technology, Brisbane, QLD 4000, Australia
[2]Centre for Robotics, Queensland University of Technology, Brisbane, QLD 4000, Australia
[3]The Prince Charles Hospital, Brisbane, QLD 4032, Australia

Corresponding author: Anjali Tumkur Jaiprakash (anjali.jaiprakash@qut.edu.au)

This work was supported in part by the Advanced Queensland Scheme, and in part by the Queensland University of Technology Research Training Program.

ABSTRACT Robotic-assisted surgical procedures have recently increased in popularity in clinical environments. Applications of clinically approved surgical robots range from minimally invasive surgery to open joint replacements. In hip and knee orthopaedic procedures, access to leg joint cavities require constant manipulation of the patient's leg to a high degree of accuracy to reduce surgical injuries. This study develops a nine degree of freedom serial kinematic model of the human leg, using the well known Denavit Hartenberg Parameters, for robotic-assisted leg manipulation during orthopaedic leg surgery. The proposed model is validated through human cadaver experiments with an optical tracking system used as ground-truth to measure the leg pose. The knee and foot workspace for the model determines the pose of the leg and in comparing it to cadaver leg position. The positional error relative to the cadaver leg was found to be 0.43mm and 0.4mm respectively, with a maximum uncertainty of 3.51mm in the foot position. It demonstrates that the proposed model provides an accurate representation of the human leg motion for automated leg manipulation during orthopaedic surgery.

INDEX TERMS Joint pose analysis, medical robotics, DH parameters, anatomical measurement, measurement uncertainty.

I. INTRODUCTION

Joint surgeries are ergonomically challenging for surgeons, who are required to perform a multitude of complex physical and intellectual tasks simultaneously. For minimal invasive surgeries (MIS) such as knee arthroscopy, the surgeon needs to infer the three-dimensional internal structures from a two-dimensional video stream as shown in Figure 1b, while concurrently using both hands to steer the arthroscope and surgical instruments. It is therefore common during orthopaedic joint surgeries for surgeons to reach their mental and physical limits. It is estimated that annually more than 4 million knee arthroscopies are performed worldwide; equating to a $16 billion per year industry [1]. However, it is common for patients to suffer from significant iatrogenic damage due to surgery. Jaiprakash *et al.* showed that for knee arthroscopies, one in ten patients have a 49.5% chance of cartilage damage as a result of the surgery [2]. Robotic technologies, such as using automated leg manipulation, can be leveraged to alleviate the surgeon's workload and increase surgical precision, resulting in better outcomes for patients.

(a) A prototype of a patented Medical Robotic leg manipulator (Patent No. 2019900476) positioning a cadaver leg.
(b) Surgeon using his body to move a cadaver's leg, while watching the screen and positioning the instruments.

FIGURE 1. **Leg positioning with a robotic manipulator (1a) and surgeon (1b) during cadaver experiments.**

The associate editor coordinating the review of this manuscript and approving it for publication was Yang Tang.

To automate the manipulation of the human leg during surgery, a robotic manipulator needs to 'know' how to manipulate the leg safely and accurately into a position, suitable for surgery. The importance of leg motion is demonstrated during a knee arthroscopy, where the surgeon sets the leg angles (Figure 1b), by moving the patient's foot to a specific position, to create a gap inside the knee to allow the entry of surgical equipment [3].

Based on the information from the inside of the knee joint [4], a surgeon determines the hip and knee joint angles, to change the instrument gap for surgical access [3]. For an automated leg manipulator robot to set the correct joint angles to produce the internal knee geometry during surgery, the desired real-time foot positional information is required to move its end-effector to that position (Figure 1a).

The human leg, as used in this study, starts from the femoral ball joint at the hip and extends to the sole of the heel, including the knee. From the hip to the heel, the leg has twenty-one degrees of freedom (21DOF) – three in the hip ball joint, six in the knee, six in the talocrural joint and six across the subtalar joint (effectively 12DOF across the ankle joint complex (AJC)) [5], [6]. Each of these variables can be manipulated or locked to control parts of the leg to enable a specific internal knee joint geometry to satisfy the requirements for certain surgical procedures. If we treat the leg similar to a robot arm with the end-effector the foot (note, this is different to the previously mentioned manipulator's end-effector), traditional robot principals can be used to relate the desired joint angles to an end-effector position. To control the motion of the 3DOF in the hip [7] and 6DOF in the knee [8] for automation, the pose of the leg must be known.

The robot arm pose can be defined by kinematic models, such as the screw or DH Parameter models. A robotic model of the human leg will support setting hip and knee joint angles during surgery, without a need for tracking systems to be installed on a patient's leg. Kinematic models are mainly used in robotic applications where a forward kinematic model provides the position of an end-effector. In contrast, inverse kinematics used the end-effector position to calculate the joint angles [9]. Once the desired joint angles are known, the forward kinematics model of the leg can be used to determine the foot position. With the leg manipulator attached to the patient, the inverse kinematics model of the manipulator (not part of this study) will action its movements to set the patient's foot and knee in the position as specified by the leg model.

Current research in kinematic models for robotic applications targets specific joints [10], motion in a specific plane [11], or if the complete leg is considered then only a 6DOF model is used for the implementations of the leg [12], [13, p. 245]. Most humanoids use a one DOF hinge model for the knee [14] as shown by Joukov *et al.* [15]. However, in the medical environment, surgeons require a high-fidelity model which utilises all the degrees of freedom in specific areas of the leg to perform complex manoeuvres. During leg joint surgery, the relative motion between variables such as abduction and internal rotation in relation to flexion angles is required to manipulate a patient's leg to gain access to the internal knee [16]. One example used throughout this study is knee arthroscopy, where 3DOF at the hip and 6DOF in the knee are used at different times during the surgical procedure.

To infer the required foot position for the desired leg joint angles during surgery, this study develops a novel 9DOF model of the human leg, using the industry-standard DH parameters. The model uses pre-operative Computed Tomography (CT) scan data for patient-specific customisation to enhanced accuracy. As detailed by Bruyninckx *et al.* [17], the magnitude of the uncertainty is parameterised by the unknown joint angle errors. The Joukov *et al.* 1DOF model of the knee obtained an uncertainty of 5.03^o in the flexion error. There were no models found in the literature that intent to replace optical tracking as used in the Mako system or to improve joint information. Using CT scan information it was possible to accurately identify the geometry of the individual leg parameters (such as femur or tibia lengths), which refine the model and improve the accuracy to align closely with the ground-truth kinematic model, where the actual knee and foot positions are measure using optical tracking. The proposed model is verified using cadaver experimentation with an optical ground-truth system.

A. PROBLEM DESCRIPTION

During knee arthroscopy, the leg must be positioned in a particular configuration for each of the surgical phases [13, p. 245]. This configuration is determined by the required joint angles to produce a favourable internal joint geometry for surgical access to different parts of the knee [8]. Although previous studies and solutions utilise mechanical markers screwed into the bone [18], it is desirable to achieve the correct leg configuration without these invasive markers autonomously, and during minimally invasive surgeries have internal joint information available to minimise iatrogenic damage.

Therefore, this article sets out to define a DH model for the human leg suitable for robotic manipulation during knee arthroscopy, without the need for invasive markers [19]. The contributions of this study are:

1) Develop a 9DOF DH Parameter model of the human leg.
2) Determine the model knee and foot position error with that of a comparison with a cadaver leg, which used a ground-truth optical tracking system.
3) measure the uncertainty in the model due to measurement errors.
4) Validates the model against a cadaver leg workspace.

As aforementioned, the objective of this model is to take as input the desired leg joint angles, to infer then (through the kinematic model) the end-effector position required to achieve these angles.

II. PROPOSED 9 DOF KINEMATIC MODEL OF THE HUMAN LEG

As aforementioned, the proposed kinematic model of the hip and knee will allow the use of a leg manipulation robot

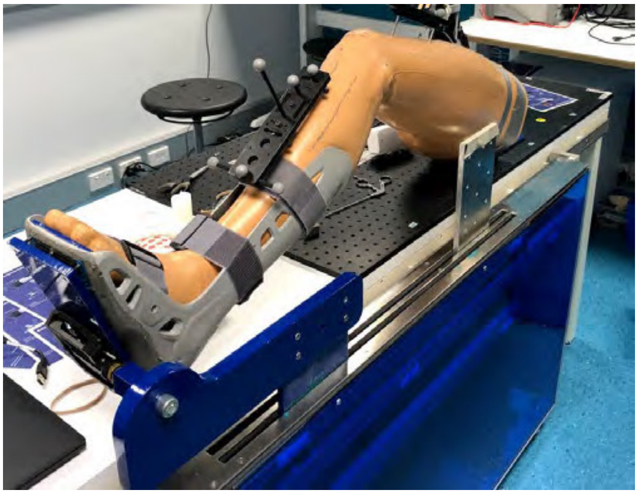

FIGURE 2. **Leg Manipulator robot developed for leg surgery (Patent No. 2019900476). The position of the foot determines the pose of the knee and hip joints. The robot model of the leg provides the coordinates of the foot to the robot, and using the robot's inverse kinematic model the foot can be placed into that position.**

to automate leg movements and joint positions. To increase surgical space and reduce interference with the surgery, the patient's foot is used as a grip point to manipulate the 9 degrees of freedom (DOF) [13, p. 245] of the hip [7] and knee motion [8] as shown in Figure 2, with the prototype surgical bed-attached robot (Australian Provisional Patent No. 2019900476) manufactured during this study. When automated, the manipulation system will identify and measure the instrument gap [3], and determine the leg pose to set the correct gap. Using the DH parameter model, the new foot position is calculated from the pose, and the manipulator moves the leg to that position, which sets the required leg pose.

A. BACKGROUND

1) DH MODEL

Several robot kinematic models exist. A popular kinematic model is the Denavit and Hartenberg (DH) model, that was developed by Richard Hartenberg and Jacques Denavit in 1955, with a unique notation to describe a serial robot's joints and links [20]. The DH model is today well-known and has been used to define many robot arms over the years. Alternative robot arm modelling systems exist and have benefits and drawbacks relative to the DH notations. It is essential to represent a leg kinematic model in a known format. A Cartesian Joint Coordinate System (JCS) was developed in 1983 by Grood and Suntay [21]. It is the recommended knee model JCS by the International Society of Bio-mechanics and will be used in this study to model the knee joint. Pennock and Clark [22] compared three models – Grood and Suntay compared to Lafortune [23] and Genucom [24] and found them similar in accuracy. The model developed in this study use the Grood and Suntay model principals; however, we use 6DOF for the knee and changed from the basic rotations to the widely used DH Parameter robot model. Frank Park shows that the product–of–exponentials (POE) system has some advantages over the DH parameters; however, the DH parameters is an industry-standard [25]. Indeed, the DH parameters are used by many engineers and popular robot configurations, supporting future integration with the leg kinematic model. Wu *et al.* developed an analytical approach to convert from POE to DH parameters to support the use of robots defined with the POE system [26]. Fujie *et al.* used the Grood and Suntay JCS and developed a 6DOF inverse kinematic model of the knee for using advanced testing devices on the knee [10]. Their model only included the knee and is used primarily for leg-attached devices to simulate knee kinematics. They tested the forces on the knee joint and used externally measured forces to verify the model. The model they developed is shown to be accurate, and the same JCS configuration will be used as part of the model in this study. The DH parameters in this study will be different from the Fujie *et al.* model due to the addition and integration of the hip to the overall solution and addition of the measurement uncertainties in the model [10]. However, they have shown the knee model to be accurate and this study will develop the overall leg model and will only show the knee translation accuracy at a specific point to verify the overall model.

For knee and hip surgery, the patient's foot is manipulated to adjust the joint kinematics to achieve a surgical position and to ensure seamless integration with many other robots and applications [10]. The standard DH parameter model will be used in the robot pose model developed in this study [27]. The notation represents the geometric configuration of each link and joint of the leg completely with four DH parameters variables (α, θ, d and a) [9]. With the DH parameters known between two link frames, the homogeneous transformation can be calculated, and with all nine sets of link parameters identified, the final position of the foot can be calculated for any joint configuration relative to the base position.

2) LEG MECHANICS

Table 1 shows the ranges for active manipulation (such as for a cadaver leg) or under passive conditions. These ranges will not only influence limitations set during the implementation of the kinematic model but govern forces from robotic manipulation not to exceed or alter the joint's natural motion. Flexion or extension is the primary movement of the knee in the sagittal plane, with the centre of rotation on the femur and the typical range from $0\,^{\circ}$ to $120\,^{\circ}$ [28]. During extension, hyper-extension can occur that extends the tibia slightly more than a straight leg (normally to $-5\,^{\circ}$) [29]. Posterior / Anterior translation was observed by Hill *et al.* that showed that in the sagittal plane, the femur rolls and slides on the tibial plateau during flexion [30]. Iwaki *et al.* and Johal *et al.* measured cadaver knees using an MRI to show that for passive knee flexion, there is an internal rotational motion through the sagittal plane of the tibia [31], [32]. At any point up to $90\,^{\circ}$ the tibia can achieve internal rotation without flexion in the normal kinematic range [33]. Active rotation of the tibia (such

TABLE 1. Passive (loaded) ranges for the knee, and hip joints [8], [28], [29], [32], [33], [35], [36], [36]. Movement of the hip and knee depends to different degrees on the flexion in the specific joint as shown in column two.

Movement	Dependency on Flexion	Range [±15%]
Hip Rotations		
Hip Flexion \ Extension		-16° - 120°
Hip Adduction \ Abduction	at 90°	-12° - 39°
Hip Internal / External	at 90°	8°
Knee Rotations		
Flexion \ Extension	Negligible	-5° - 160°
Internal / External	Flexion (F): -5°	0°
	F: -5°to 20°	10°
	F: 10°to 30°	10°
	F: 20°-160°	18°
	Flexion at 90°	20° to 30°
Varus / Valgus	F: 20°-120° - Varus	8°
Knee Translations		
Anterior / Posterior	F: -5° to 0°	0mm
medial Condyle	10° - 30°	-1.5 mm
medial Condyle	-5°-120°	3.4 mm
medial Condyle	120°-160°	8.4 mm
lateral Condyle	-5°-120°	21 mm
lateral Condyle	120°-160°	9.8 mm
Medial / Lateral	F: 0°- 30°	1 - 2mm
	F: 30°-120°	0
Proximal / Distal	F: 0°	2 - 5mm
	F: 0°-20°	0 - 2mm
	F: 20°-120°	Minimal

as during surgery) can limit and even reverse the natural rotation from 90° to 10°. During extension, a screw home mechanism is initiated for the final 10° to stabilise the knee joint [28], [31] and limiting movement and surgical access to the internal knee [33]. In the coronial plane medial to lateral rotation (varus-valgus force) pivots the tibia sideways relative to the femur, resulting in knee abduction or adduction [34]. Flexion below 10° restricts varus-valgus (and most other) motion, locking the leg and limiting access to the internal knee for surgical application [8]. Medial to lateral translation and distraction and compression between femur and tibia is minimal during passive flexion [8] and not a significant factor during some surgeries such as knee arthroscopy.

B. ASSUMPTIONS

In developing the kinematic leg model the following assumptions are made:

1) The leg was modelled as a serial robot, however a model can be setup with a combination of serial and parallel links.
2) The hip joint is modelled as perfect ball and socket joint and the knee joint as rotational and translation motions.
3) The limited range and angle combinations of the human leg mitigate singularity issues.
4) The DH Parameter model convention can be "standard" or "modified". This study uses the standard DH Parameter convention.
5) The ankle joint complex is locked for robotic manipulation and it is assumed that this joint is rigid.

TABLE 2. Notations used in this study [9], [19].

Abbreviation	Description
c_θ	$\cos\theta$
s_θ	$\sin\theta$
Frame	Coordinate system at a point
$\boldsymbol{T}$	Transformation Matrix
${}^{D}\boldsymbol{R}_B$	Rotation Matrix of frame B relative Frame D
$\boldsymbol{v}$	A vector
$\hat{v}$	A unit vector
${}^{B}\boldsymbol{a}$	Vector from frame B to Point A
${}^{B}\tilde{\boldsymbol{a}}$	Point A (homogeneous) relative to Frame B
$\mathcal{M}$	Frame M
X,Y,Z	Coordinate axes of World frame
x_c, y_c, z_c	Coordinate axes of local frame $\mathcal{C}$
ψ	Hip Varus angle (x-z plane)
θ	Hip Flexion angle (y-z plane)
Γ	Hip Roll angle (x-y plane)
β	Knee Varus angle (x-z plane)
α	Knee Flexion angle (y-z plane)
γ	Knee Roll angle (x-y plane)

C. NOTATION AND TERMINOLOGY

The notation for the transformations, vectors, positions, poses and axes as used in this document are adapted from Peter Corke's 'Robotics, Vision & Control' [9] and the joint angles as calculated in Strydom *et al.* [19], are summarised in Table 2. Medical specific terminology is detailed in McKeon *et al.* [37]. The hip angles are relative to the global body frame $\mathcal{W}$, while knee angles are relative to the femur frame $\mathcal{C}$.

D. THEORY

Our proposed derivation models both the hip and knee joints. For each of the joints we first discuss its mechanics related to Figure 3, which supports the kinematic structure defined in Figure 4.

The hip has 3DOF [7] as shown in Figure 3 and using robotic principals we can model this joint using three revolute joints (θ_2, θ_3 and θ_4) as illustrated in Figure 4. The hip joint and femur are connected by the femoral neck, changing the rotational aspects of the leg and extending the range of motion of the hip [38]. The femoral neck ($\vec{f_h}$) offsets the femur anatomical axis ($\vec{v_{fa}}$), however, leg motion is described along the mechanical axis ($\vec{v_f}$):

$$\vec{v_f} = \vec{v_{fa}} + \vec{f_h} \tag{1}$$

The offset of the femur relative to the hip ball and socket joint, changes the motion of the leg in relation to the hip joint: Hip ball socket internal rotation results in flexion of the femur

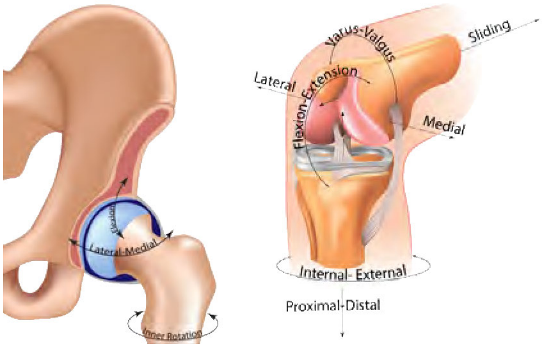

(a) 3DOF of the Hip [41] (b) 6DOF of the knee [8], [16]

FIGURE 3. Hip and Knee Joints.

TABLE 3. DH Parameters for a 9 DOF leg with hip and knee links as shown in Figure 4. Each link is defined as either a rotation (R) or translation (T).

Link	Type	Variable	DH Parameters θ_i	d_i	a_i	α_i
1	T	Body Align	$\frac{\pi}{2}$	q1	0	$\frac{\pi}{2}$
2	R	Hip Flexion	q2	0	0	$\frac{\pi}{2}$
3	R	Hip Varus	q3	0	0	$\frac{\pi}{2}$
4	R	Hip Rotation	q4	L4	0	$\frac{\pi}{2}$
5	R	Knee Flexion	q5	0	0	$\frac{\pi}{2}$
6	T	Knee Sliding	$\frac{\pi}{2}$	q6	0	$\frac{\pi}{2}$
7	R	Knee Varus	q7	0	0	$-\frac{\pi}{2}$
8	T	Knee Med/Lat	$-\frac{\pi}{2}$	q8	0	$-\frac{\pi}{2}$
9	T	Knee Gap	0	q9	0	0
10	R	Knee Rotation	q10	L10	0	0

in the sagittal plane, which is the main motion during walking [39]. Hip socket anterior motion translate to femur internal rotation and is limited by the hip socket configuration [40]. Hip socket proximal motion is equivalent to the femur lateral motion [38].

The knee joint has 6DOF, three rotations and three translations [16], as detailed in Figure 3b. It allows sufficient manipulation for surgical applications and has been extensively studied to determine the kinematic properties and planes each occurs in [42]. As shown in Figure 4 the knee can be modelled using three revolute (θ_5, θ_7 and θ_{10}) and three translational joints (d_6, d_8 and d_9).

From the model as shown in Figure 4, the leg configuration has nine parameters between the hip and knee joints that is needed for development of the DH parameter model, which can be calculated for each of the links. For both the femur and tibia the mechanical axes are used for leg motion to develop the model. For the DH parameters each link (i) has the following characteristics: offset a_i and joint angle θ_i is the z-axis positional and angular displacement, while the the offset d_i and link twist α_i are the x-axis positional and angular displacements, respectively [43].

Each link is individually assessed against the DH Parameter rules [9] to provide an end-to-end combination. The complete DH Parameters list for the human leg (ankle locked) that include each of the 9 links as shown in Figure 4 are

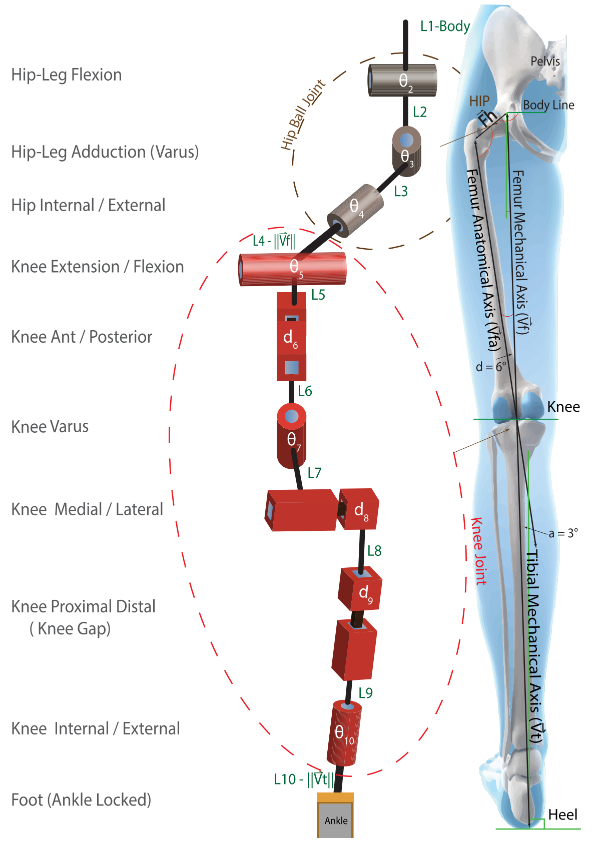

FIGURE 4. Leg Robot Model showing the model on the left with the variables for the hip and knee joints. The leg on the right side shows for the femur the mechanical ($\vec{v_f}$) and anatomical $\vec{v_{fa}}$ axes and for the tibia the mechanical axis ($\vec{v_t}$), which is equivalent to the tibial anatomical axis.

detailed in Table 3. For a straight leg the q values (joint variables) are: $[0\ \frac{\pi}{2}\ \frac{\pi}{2}\ \frac{\pi}{2}\ \frac{\pi}{2}\ 0\ 0\ -\frac{\pi}{2}\ 0\ -\frac{\pi}{2}]$. A homogeneous matrix (A matrix) that details the transformation from the link coordinate frame $i-1$ to link frame (i) can be expressed using the standard DH parameters as detailed in Table 3 such that [9]:

$$^{i-1}\boldsymbol{A}_i = \begin{bmatrix} c_{\theta_i} & -s_{\theta_i}c_{\alpha_i} & s_{\theta_i}s_{\alpha_i} & a_i c_{\theta_i} \\ s_{\theta_i} & c_{\theta_i}c_{\alpha_i} & -c_{\theta_i}s_{\alpha_i} & a_i c_{\alpha_i} \\ 0 & s_{\theta_i} & c_{\alpha} & d_i \\ 0 & 0 & 0 & 1 \end{bmatrix} \tag{2}$$

The pose of the foot (or ankle, which is used in this study as the foot position) is approximately equal to the homogeneous transformation, which can be expresses as a product of the A matrices:

$$\boldsymbol{T}_f = \prod_{i=1}^{I} {}^{(i-1)}\boldsymbol{A}_i \tag{3}$$

where I=10, the number of links for the model of the leg as detailed in Table 3 [9], [27].

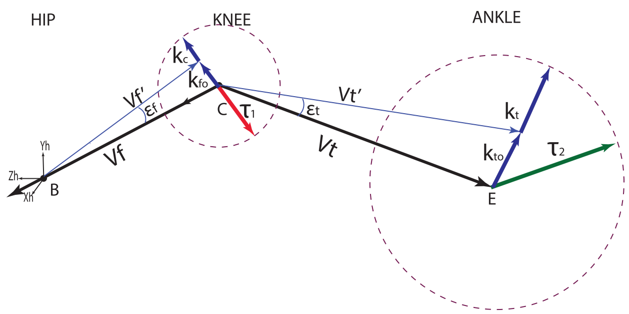

FIGURE 5. Maximum measurement errors of the hip joint (τ_1), and combined hip and knee joints (τ_2) mechanical vectors.

The output format of the pose of the model foot is a homogeneous matrix $\boldsymbol{T}_f$ in the format:

$$\boldsymbol{T}_f = \begin{bmatrix} r_{11} & r_{12} & r_{13} & r_{14} \\ r_{21} & r_{22} & r_{23} & r_{24} \\ r_{31} & r_{32} & r_{33} & r_{34} \\ 0 & 0 & 0 & 1 \end{bmatrix} \quad \in \quad \boldsymbol{SE(3)}; \tag{4}$$

Finally, to derive each element of the matrix (4), we use the A matrices (2) in (3) to calculate each element of the matrix $\boldsymbol{T}_f$.

1) UNCERTAINTY

As aforementioned, surgical applications demand accurate leg motion. However to determine the validity of using a robot model, the maximum uncertainties in the DH Parameter model foot position, needs to be taken into account.

For the model, the optical tracking and CT measurement errors, as well as the knee joint translations determine the end-effector (foot) uncertainty as shown in Figure 5. The maximum model foot positional error ($\boldsymbol{e}_{max}$) that can be expected is:

$$\boldsymbol{e}_{max} = \boldsymbol{\tau}_1 + \boldsymbol{\tau}_2 - k_{ts_{max}} \tag{5}$$

where $\boldsymbol{\tau}_1$ is the maximum translation error vector due to the hip measurement errors, affecting the knee position, $\boldsymbol{\tau}_2$ the maximum translation difference vector due to the knee measurement errors and $k_{ts_{max}}$, the femoral sliding as detailed in Table 1 that affect the foot position. We define $\boldsymbol{\tau}_1$ as:

$$\boldsymbol{\tau}_1 = \|\boldsymbol{k}_f o\| + \|\boldsymbol{k}_c\| \tag{6}$$

$\boldsymbol{k}_c$ is the CT scan measurement error and $\boldsymbol{k}_{fo}$ the translation error at the knee due to errors in the the hip joint rotations. From Figure 5:

$$\boldsymbol{k}_{fo} = \boldsymbol{v}_f' - \boldsymbol{v}_f \tag{7}$$

with

$$\boldsymbol{v}_f' = R_e \boldsymbol{v}_f \tag{8}$$

where, using the xyz rotational convention, $R_e \in \boldsymbol{SO(3)}$ is the rotation error matrix [44] for both the femur and tibia,

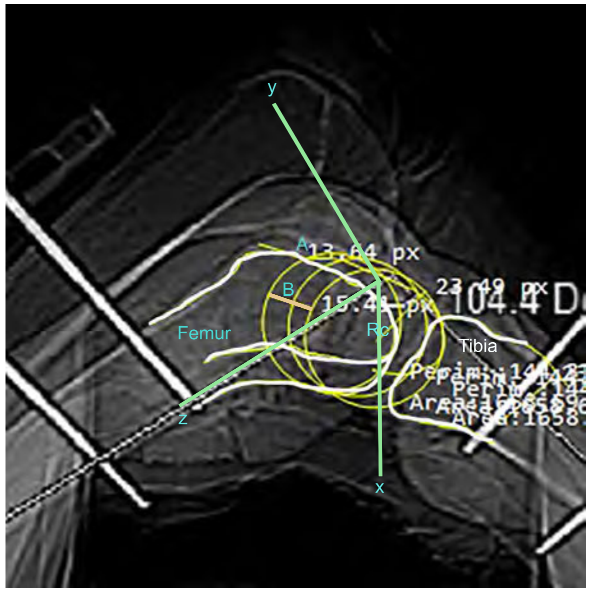

FIGURE 6. CT Scan of knee at 86^o. the tibia roll and slide on the femur (white) and the translation (yellow) of 14.5mm is shown from the translated centre of rotation relative to the femoral frame (green).

constructed from the maximum optical measurement errors, α, β and γ:

$$\begin{aligned} \boldsymbol{R}_e &= \boldsymbol{R}_{ex}(\alpha)\boldsymbol{R}_{ey}(\beta)\boldsymbol{R}_{ez}(\gamma) \\ &= \begin{bmatrix} c_\beta c_\gamma & -c_\beta s_\gamma & s_\beta \\ s_\alpha s_\beta c_\gamma + c_\alpha s_\gamma & -s_\alpha s_\beta s_\gamma + s_\alpha c_\gamma & -s_\alpha c_\beta \\ -c_\alpha s_\beta c_\gamma + s_\alpha s_\gamma & c_\alpha s_\beta s_\gamma + s_\alpha c_\gamma & c_\alpha c_\beta \end{bmatrix} \end{aligned} \tag{9}$$

As a result, ϵ_f, the femur angular error have a translation error at the knee of $\boldsymbol{k}_{fo}$ as shown in Figure 5. In this instance $\boldsymbol{\tau}_1$ does not depend on any internal joint translation as the hip is modelled as three rotations, however the CT measurement error ($\boldsymbol{k}_c$) increases the translational error at the knee.

For robotic manipulation, the ankle joint is locked and we assume it to be rigid. The translation difference at the foot relative to the knee position, are due to measurement errors in the knee joint and natural knee translation, such that:

$$\boldsymbol{\tau}_2 = \|\boldsymbol{k}_t\| + \|\boldsymbol{k}_{to}\| \tag{10}$$

The knee error include the translation difference $\boldsymbol{k}_t$ and optical measurement rotation errors $\boldsymbol{k}_{to}$ as shown in Figure 5. With $\boldsymbol{k}_{xz}$ the knee flexion and medial /lateral and proximal / distal translations and $\boldsymbol{k}_c$ the CT scan measurement error:

$$\boldsymbol{k}_t = \boldsymbol{k}_s + \boldsymbol{k}_{xz} + \boldsymbol{k}_c \tag{11}$$

The knee rotational error is an angular error of ϵ_t which results in a translation error $\boldsymbol{k}_{to}$, with:

$$\begin{aligned} \boldsymbol{k}_{to} &= R_e \boldsymbol{v}_t - \boldsymbol{v}_t \\ &= \boldsymbol{v}_t(R_e - 1) \end{aligned} \tag{12}$$

Because the translations inside the knee are small relative to the leg dimensions, we have set the knee translations initially

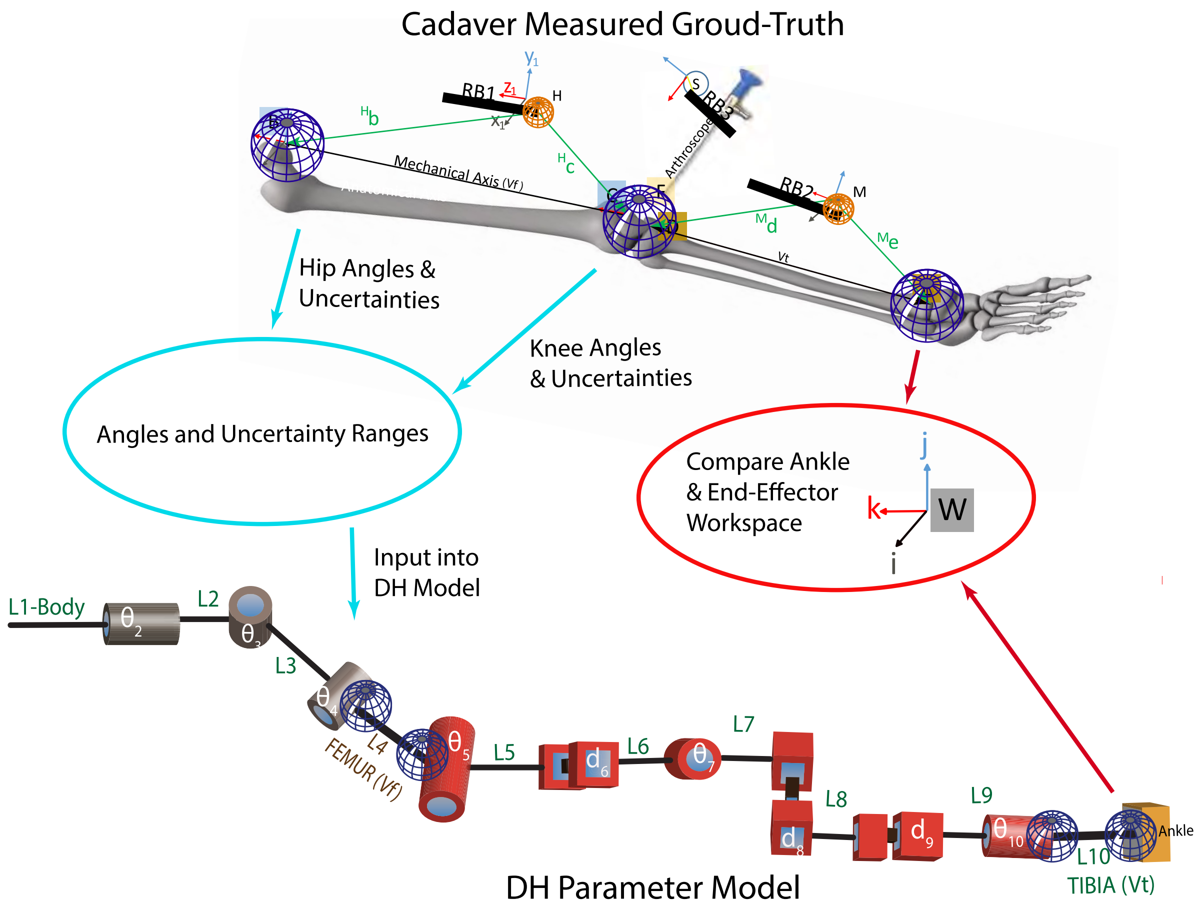

FIGURE 7. Comparing the measure joint angles and translations to the model output. CT measurement errors are shown with the spheres for both the ground-truth and model. The optical measurement system is detailed in [19], using the rigid bodies (RB1-3). Angles calculated from the cadaver leg are input into the model and the resultant foot and model end-effector compared to determine the model accuracy.

to zero in validating the DH Parameter model against the cadaver leg. These translation will be seen in the model as part of the foot positional difference and the foot positional error will be shown at a point (86.6°). The total translation difference in the knee (k_t) is thus not only due to the CT measurement errors $\boldsymbol{k}_c$, but also natural translation inside the knee, which include sliding ($\boldsymbol{k}_s$) due to flexion and medial /lateral and proximal / distal translations ($\boldsymbol{k}_{xz}$) as detailed in Table 1. Sliding is the largest translation in the knee joint during motion with a range from 0mm at 0^o and a maximum of 21mm when fully flexed. Using a CT scan as shown in Figure 6 the sliding at 90^o was measured as 14.5mm.

III. KINEMATIC MODEL VALIDATION

The model is verified by moving it with the same rotations and translations measured during cadaver surgery, where range limits are naturally imposed. The accuracy of the workspace of the cadaver and model will be compared with each other, as shown in Figure 7.

A. EXPERIMENTAL SETUP

A Stryker arthroscopy system was used to capture images of the knee gap. The video frame rate for the arthroscope camera is 60 frames per second, with the full resolution of the video frames 1280 × 720. An OptiTrack optical tracking system was setup with ten Flex 13 cameras and 14.7mm optical balls. Two cameras were set up in video mode and eight to track the optical markers. The OptiTrac systems are sampled at 120 frames per second, and the leg movement was sustained for 3.58 minutes, supporting 33000 samples for comparison. Against each sample, the hip and knee angles (as measured in [19]) are input into the DH model and configured in Matlab vR2018b using Peter Corke's toolbox [9]. The foot (anatomical ankle positions) are compared between the Matlab output of the model and the measured cadaver values, as shown in Figure 7, to determine the accuracy of the model.

B. JOINT ANATOMICAL REFERENCE

The anatomical positions are determined inside the leg using the optical and CT measurement information, which is used to set up the mechanical axes of the femur and tibia, as shown in Figure 8a. For validating the DH model, the following anatomical points inside the leg were used:

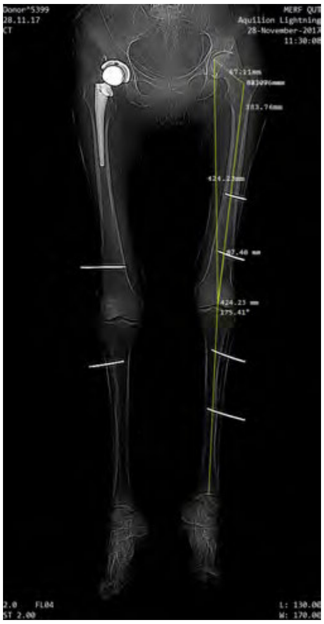

(a) Femur Anatomical and mechanical axes.

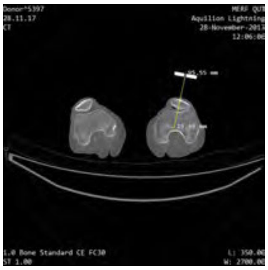

(b) Measurement from G to femoral Condyle Centre.

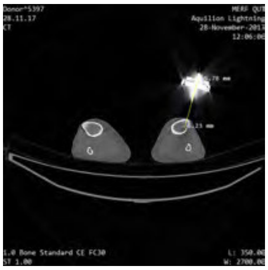

(c) Measurements from RB plate and surgical pin to tibia centre.

FIGURE 8. CT Scan of two cadaver limbs (a) and cross-section scans of the femur at condyle centre (b) and at the surgical pin.

- The condyle centre on the femur (Figure 8b) where the centre of the condyles starts to form (using the CT scan slices)
- Hip ball joint centre - where the femoral mechanical axis intersects the ball joint centre as shown in Figure 8a
- Tibia top as shown on the tibia mechanical axis in Figure 4
- Centre of the ankle joint (Figure 4) on the intersection of the tibial mechanical axis and the tibia (Figure 8c) at the AJC. Through this study, this position is referred to as the foot position

From these anatomical positions, the mechanical vectors $\boldsymbol{v}_t$ and $\boldsymbol{v}_f$ are defined that are used to calculate the hip and knee angles. Vectors can be defined inside the knee between any two anatomical points to determine the knee translations at that point.

C. WORKSPACE

To validate the robotic kinematic model of the leg, the workspace of a cadaver knee and foot is compared to that of the model as shown in red in Figure 7. Specific combinations of the model (procedure dependent where we use only specific links in the DH model and set the others to zero) change the workspace. Surgeons extend a patient's hip, knee or foot to create space for instruments and to gain access to areas to operate on – these manoeuvres typically reach maximums for specific parts of the model. However, others are not used - for example, during hip surgery, the knee joint is manipulated but not the ankle. Walking, jogging and different sports activities use different parts of the leg again; however, in contrast to surgical manoeuvres, these activities rarely reach the maxima of the joints' motion ranges. For this study, the entire workspace of the leg with the three DOF in the hip and the six DOF in the knee will be compared using the kinematic model developed, with data from cadaver experiments as input parameters as shown in blue in Figure 7.

To compare the knee and foot workspace, the model and the leg parameter ground-truth as discussed in the Section III-E, are both configured in Matlab using the Peter Corke toolbox [9].

The model workspace is validated through:

1) Using ranges from the passive research of the hip and knee joint, which is adjusted to the cadaver using the CT Scan information. Using an optical tracking system, markers were mounted on the cadaver leg as detailed in Figures 8a and 9a. Angles for the hip were calculated from the tracked markers and input into the DH model of the human leg.
2) Comparison with a cadaver leg moved through a range of surgical positions for the hip and knee joints and measured using an OptiTrack system. Angles from measured data are calculated and input into the kinematic model to measure the knee and foot (ankle point) workspace and positional error.

TABLE 4. Experiments to measure a cadaver leg using CT Scan and optical tracking and move the cadaver leg through a range of motions to measure the workspace of the knee and foot positions.

Experiment	Cadaver	Sex	Age
Cadaver Measurements	L/R Knees	Male	60-70
Kinematic Tests	L/R Knees	Female	50-60

D. CADAVER EXPERIMENTS

Ethical approvals were gained for the three Cadaver experiments; using four legs; as detailed in Table 4 and conducted at the Queensland University of Queensland's Medical Engineering Research Facility (MERF) located on the Prince Charles Hospital campus in Brisbane, Australia. For Cadaver experiments, special rigid bodies and optical marker patterns were developed to ensure alignment with the cadaver femur and tibia, enabling accurate calculation of all knee and hip rotations and translation ([19]. CT scans of each cadaver leg were taken and used to analyse the position of the anatomical points, which can be used to compare to the model and cadaver knee and foot positions.

E. MEASUREMENT OF CADAVER JOINTS

The cadaver anatomical positions are measured as detailed in [19] and the joint parameters calculated. During the experiment, the cadaver leg is moved manually, as shown in Figure 9b to cover a wide spectrum of the workspace of the knee and hip joints. The leg is manipulated through the various joint configurations, applying significant forces on these joints to ensure that the workspace represents the typical

(a) Optical markers on the Cadaver Leg.

(b) Leg is manipulated using both the hip and knee rotations and translation during the cadaver experiment.

FIGURE 9. Capturing Cadaver leg parameters using optical tracking.

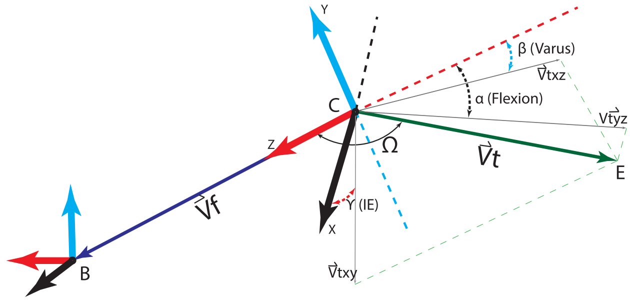

FIGURE 10. The knee angles (α, β and γ) are relative to frame C on the femoral condyle, while the hip angles are relative to the world frame at point B. Ω is the total angle between the femur and Tibia vectors.

leg motions during surgical procedures. These angles and translations are used as input into the DH model, as shown in Figure 7. The leg pose is dependent on both the knee and foot positions. The output of the model's knee and foot workspace is then compared with that measured from the cadaver with the optical tracking system.

To measure the cadaver joint parameters, the markers are set up and aligned, as detailed in 9a and 8a. The knee rotations are calculated relative to the femur frame (at the condyle centre - C) as shown in Figure 10. On the tibia, a vector ($\boldsymbol{v}_t$) is defined from the centre of the frame at the top of the tibia in the knee joint (Figure 8b) to the foot, describing the motion of the tibial mechanical axis, relative to the femur. The femur mechanical axis describes a vector ($\mathbf{v_f}$) for the hip rotations from the hip ball joint to the femoral condyle centre.

The XYZ rotational matrix as detailed in [19] is used to obtain the knee angles (α, β and γ) between vectors v_f and v_t as shown in Figure 10. The rotational matrix between the femur and tibia is [45]:

$$^{v_f}\boldsymbol{R}_{v_t} = 2\frac{(t_r t_r^{-1})}{(t_r^{-1} t_r)} - I \tag{13}$$

where $t_r = \mathbf{v_f} + \mathbf{v_t}$ and $^{v_f}\boldsymbol{R}_{v_t} \in SO(3)$. Using this rotational matrix in the $\mathbf{R} = R_X R_Y R_Z$ order, the knee angles as defined

TABLE 5. Values used for calculations [4], [19].

Value	Description
0.18^o	ϕ - the maximum optical error
(2,21,5)mm	k_s and k_{xz} - natural knee translation
$\pm0.47^o$	Uncertainty in the joint angles
379mm	$\|\|v_f\|\|$ - length of femur vector
372mm	$\|\|v_t\|\|$ - length of tibia vector
0.34mm	k_c - CT scan measurement error
14.5mm	CT scan translation of the knee in the -Y direction at 45.5^o relative to the femoral frame
4mm	Arthroscope size

in Table 2 are:

$$\alpha = \text{atan2}(^{v_f}\boldsymbol{R}_{v_t}(2,3), ^{v_f}\boldsymbol{R}_{v_t}(3,3)) \tag{14}$$

$$\beta = \text{atan2}(^{v_f}\boldsymbol{R}_{v_t}(1,3), \sqrt{^{v_f}\boldsymbol{R}_{v_t}(1,1)^2 + ^{v_f}\boldsymbol{R}_{v_t}(1,2)^2}) \tag{15}$$

$$\gamma = \text{atan2}(-^{v_f}\boldsymbol{R}_{v_t}(1,2), ^{v_f}\boldsymbol{R}_{v_t}(1,1)) \tag{16}$$

The femur mechanical axis ($\mathbf{v_f}$) is is relative to the world frame and defined as the link from the hip joint centre to the centre of the condyles on the knee as shown in figures 4 and 8a. Angles and translations are measured relative to the sagittal (flexion), coronal (varus) and transverse (knee gap) planes. From Strydom *et al.* [19] we obtain the hip motion as defined in Table 2 as:

$$\theta = \text{atan2}(^{W}\boldsymbol{R}_C(2,3), ^{W}\boldsymbol{R}_C(3,3)) \tag{17}$$

$$\psi = \text{atan2}(^{W}\boldsymbol{R}_C(1,3), \sqrt{^{W}\boldsymbol{R}_C(1,1)^2 + ^{W}\boldsymbol{R}_C(1,2)^2}) \tag{18}$$

$$\Gamma = \text{atan2}(-^{W}\boldsymbol{R}_C(1,2), ^{W}\boldsymbol{R}_C(1,1)) \tag{19}$$

Defining vectors at different anatomical positions inside the knee between the femoral condyles and tibial plateau, we can measure the joint translation between those points.

Rotations and Translations calculated from the measured OptiTrack data are used as input into the robotic leg manipulation model as shown in Figure 7 and provide the knee and foot workspaces from the model, that can be compared to the cadaver foot workspace.

IV. RESULTS

This study develops a DH model of the human leg and verifies the model workspace accuracy for surgical applications with that of a ground-truth cadaver foot workspace [19]. The full transfer matrix ($\boldsymbol{T}_f$) for the forward kinematics, developed from the DH Parameters (Table 3), is shown in Table (4). The positional data from the same cadaver experiment were used for both the ground-truth and model as a comparison as detailed in Figure 7. Cadaver parameters, measurement errors and equipment values used in calculations for both the model and ground-truth are detailed in Table 5.

A. WORKSPACE COMPARISON

Figure 11 shows the hip angles from the ground-truth model and the error between the model and the actual cadaver knee

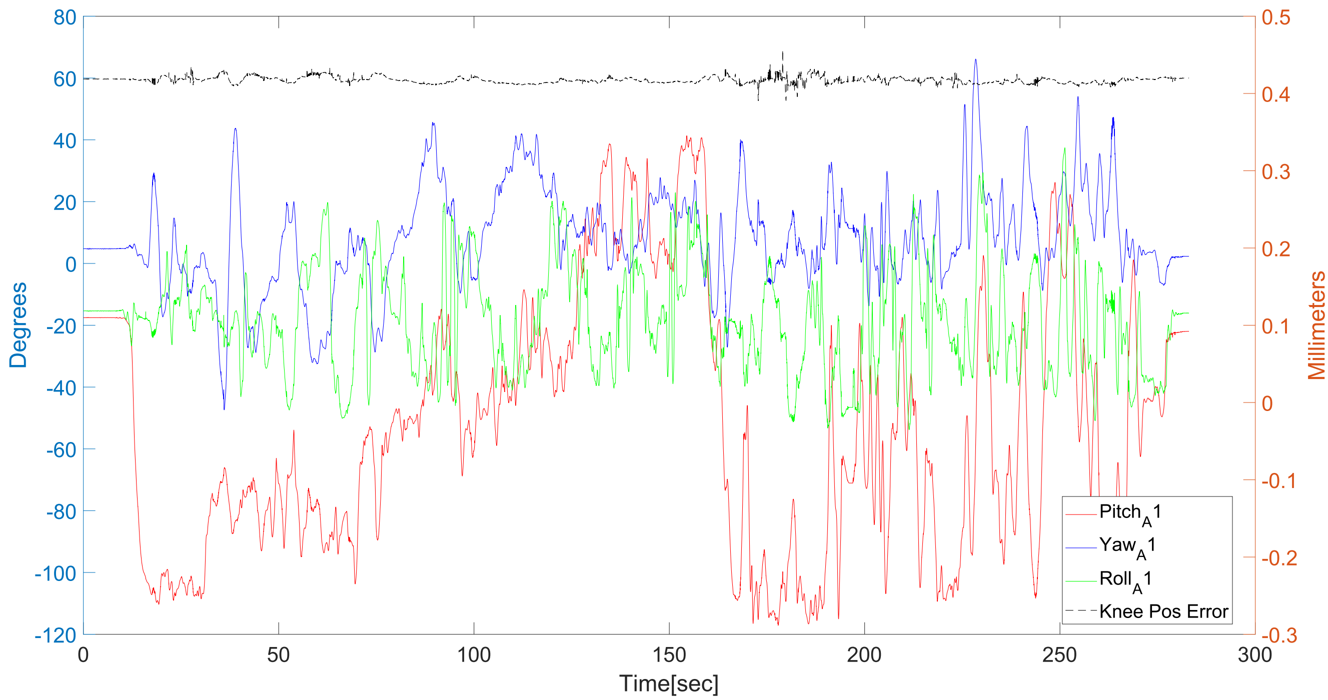

FIGURE 11. Hip Angles on the left axis and the Knee Position error on the right axis for cadaver 3397.

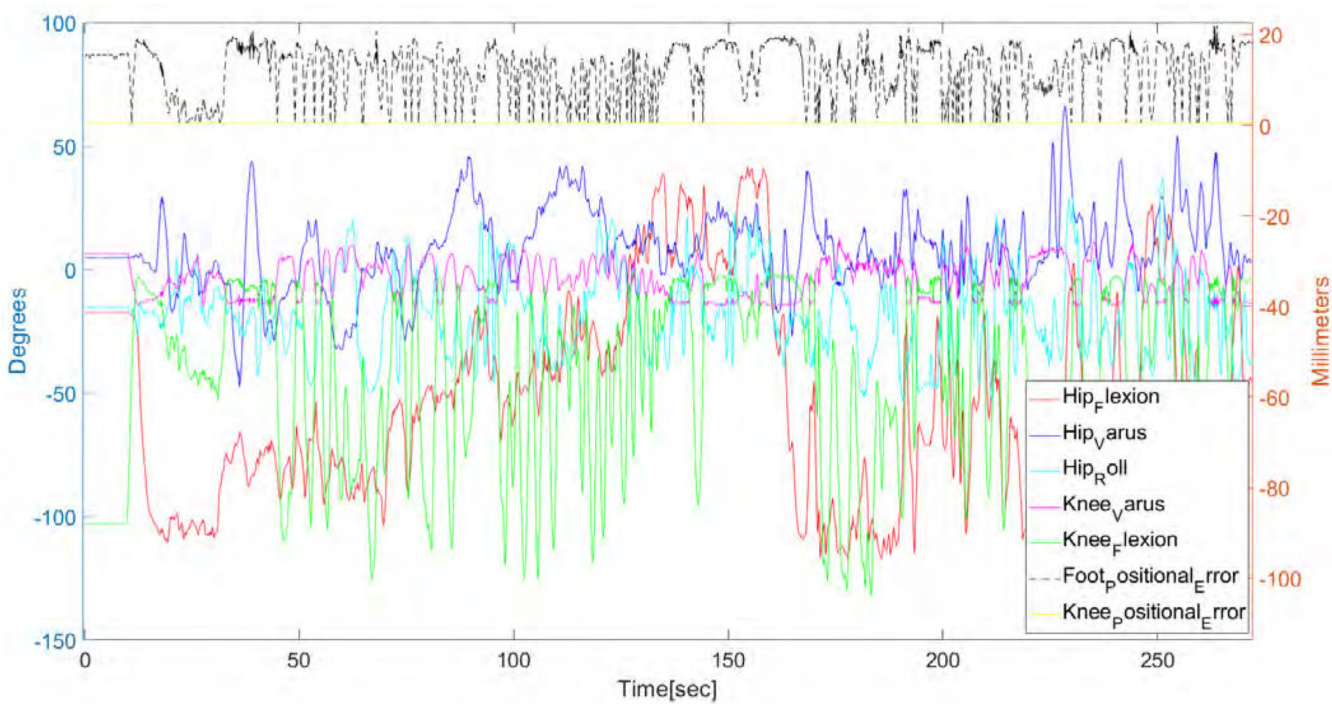

FIGURE 12. Hip and Knee Angles on left axis with foot positional difference in mm on the right axis).

position. The maximum knee position error across the data set range from 0.39mm to 0.45mm.

Figure 12 shows the knee angles and the foot positional error between the cadaver and the DH Model. The resultant positional difference as shown in Figure 12 range from 0.9mm to 22.5mm. This study does not track the cadaver knee translations in real-time, and the foot error, as shown in black in Figure 12 thus include the knee's natural translation during flexion. The foot position (end of the tibia at the ankle) depends both on the hip and knee variables. As shown in

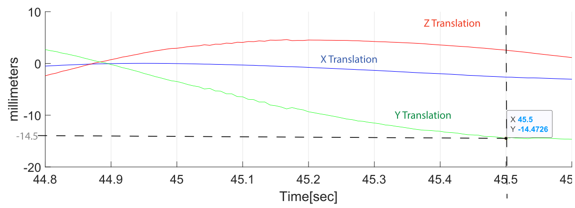

(a) XYZ Foot translation and Error in the global frame. The Y translation and error combination is -14.5mm at 45.5 seconds mm.

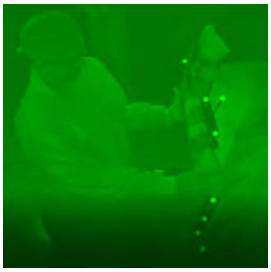

(b) Cadaver Foot at 45.5 seconds with knee at 86 degrees.

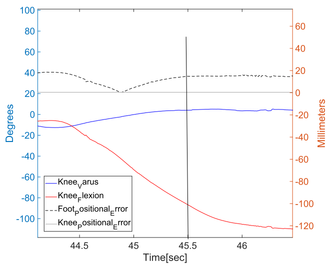

(c) Knee Angles at 45.5 seconds relative to the femoral axis.

FIGURE 13. Foot Error at 45.5 seconds and 86.6° flexion due to Knee Translation and leg error.

Figure 6 using the CT scan and in Figure 13 using motion data from the optical system that is compared to the model output, the translation inside the knee can be checked at a specific angle. Since previous research such as that by Fuji *et al.* has shown the accuracy of the knee sliding, it is not verified in real-time in this study [10], however, to show the effect of the sliding, an example at 86^o knee flexion is added to this study to verify that the accuracy of the foot error is similar to that of the knee positional error. From 0^o to 90^o if we track the motion of the centre of rotation of the tibia on the femur, the sliding of the knee k_{ts} in the -Y direction at 86^o relative to the femoral frame, is 14.5mm as shown in Figure 13. We can thus conclude the foot positional error f_{te} due to the knee at knee flexion of 86^o as shown in Figures 6 and 13 is:

$$\begin{aligned} f_{te} &= f_e - k_{ts} \\ &= 14.5 - 14.1 \\ &= 0.4mm \end{aligned} \tag{20}$$

where f_e is the foot DH model to ground-truth difference as shown in Figures 12, which is detailed in 13a and thus similar to the knee positional error results of 0.43mm.

B. UNCERTAINTY QUANTIFICATION

While in previous sections the actual errors between the model and cadaver foot were measured during leg motion, it is necessary to analyse the maximum uncertainty in the model's foot position to validate that these error values at each measured point as shown in Figures 11 and 12, all fall within the calculated foot uncertainty range.

From Section II-D1 and in (9) with the maximum angular errors: $\alpha = \beta = \gamma = \phi/\sqrt{3}$, the rotational error matrix ($\boldsymbol{R}_e$) influences the optical tracking measurement for both the tibia and femur measurements. For the calculations we used the cadaver parameter values as detailed in Table 5. In the DH Parameter model, the femur and tibia lengths are from the CT scan information, which are input into the model as shown in the bottom part of Figure 7.

Setting the internal natural knee translation ($\boldsymbol{k}_s + \boldsymbol{k}_{xz}$) to zero in the model, the translation error ($\boldsymbol{k}_t$) between the model and cadaver foot will be a maximum that include both the natural knee translation and the translations difference ($\boldsymbol{k}_c$), in the sagittal, transverse and coronal planes as detailed in (11). With the maximum translation in the knee joint as detailed in Table 5.

Using these values we determine the maximum error translation at the knee from (6), $\boldsymbol{\tau}_1 = 1.59$ and from (10), the maximum difference at the foot position as $\boldsymbol{\tau}_2 = 22.92$ and from Table 1 the maximum sliding is 21mm.

The maximum positional error between the model and the cadaver foot (e_{max}) is thus from (5):

$$\begin{aligned} \boldsymbol{e}_{max} &= \boldsymbol{\tau}_1 + \boldsymbol{\tau}_2 - k_{ts_{max}} \\ &= 1.59 + 22.92 - 21 \\ &= 3.51mm \end{aligned}$$

V. DISCUSSION

Automated orthopaedic surgery requires a full kinematic model of the human leg to manipulate and position the leg timely, safely and accurately. This research developed a nine DOF robotic kinematic model of the leg using the well known standard DH parameters. The model input (leg pose) is received from other sources, where a surgeon or external system input the required pose (angles and translations for each joint). As detailed in equation (1) and section D, the model aligns with real-life motion by using the mechanical axes and not the anatomical axes, so injuries, size, gender, or age will have little effect on the model accuracy. The mechanical axes are virtual entities, and irrespective of the cadaver can be accurately measured from the CT scan. The model thus follows normal mechanical principals to position the femoral head and foot and are not affected by anatomical differences or abnormalities. For future automated leg manipulation, the instrument gap will be monitored, and the leg pose gradually changed until the desired gap is accomplished. During each type of surgery, surgeons will use a subset of the joint variables; for example, during a knee arthroscopy, all 3DOF in the hip and four in the knee (joints 1,2,3,5,7,8 and 10 in Table 3) are used. The XYZ frame rotation [44] was used to analyse the leg pose, without any singularities as seen in Figures 11 and 12 within the limited range of the hip and knee angles. Practically during a surgery, joints that are not used are manually locked using a brace for the ankle joint complex or limiting the range of the hip or knee parameter by using bed clamps. In the model (4), the joint variables (q values) that are not used during a procedure, are set to zero to calculate the effective transfer function for that procedure.

The hip angles were measured from a cadaver leg and input into the DH model, which alters the knee position in the model. It is compared to that of the cadaver knee position at each measurement point, with the average knee positional error across the data set of 0.38mm to 0.45mm, as shown in Figure 11. It shows that the hip section of the DH parameter model is accurate for the knee position when compared to that of the optically measured cadaver knee position, and more precise than a surgeon manipulating the leg.

The foot position (end of the tibia at the ankle) depends both on the hip and knee variables. Using the knee angles measured from the cadaver knee, we compared the foot position of the cadaver with that of the model. Even though flexion of the hip and knee has the largest range of motion, other rotations such as the hip rotation can change the position of the foot significantly during flexion and thus the foot error. With the combinations of hip and knee rotations, the foot difference is 0mm to 22.5mm as shown in Figure 12, which is a combination of the hip error measured at the knee, the knee joint errors due to forces applied to the foot, and the knee's natural translation as detailed in Table 1. To determine the foot error, we measure the sliding inside the knee at 86.6°, which is 14.1mm, with the foot difference of 14.5, the foot error is 0.4mm at that point (20). The maximum foot error at 21mm sliding is 3.51mm.

A key interest for surgical applications such as arthroscopy is to position the patient's leg with precision so that the space inside the cavity where the surgical instrument is moving through is larger than the instrument ensuring no damage to the surrounding structures. With the maximum calculated DH Model foot position uncertainty of 3.51mm, the measured foot positions errors should fall within this uncertainty value as shown with the example in Figure 13, which validates the model and demonstrates that the uncertainty quantification is correct. For a tibia length of 372mm, the calculated uncertainty of 3.51mm influences the tibial mechanical axis angle (a-angle in Figure 4) accuracy by 0.01^o. Practically, this uncertainty in the mechanical axes is small if compared to the motion range and precision of the leg pose when manipulated by a surgeon.

Therefore, both measurements of the workspace or using the maximum measurement uncertainty, demonstrate that the DH model provides an accurate representation of the human leg motion for automated leg manipulation during orthopaedic surgery.

A. MODEL LIMITATIONS

Significant external forces exerted by surgeons on the leg during procedures and can slightly alter the hip socket rotational position, impacting the centre of rotation and accuracy of the results.

The robot model outputs positional information from the nine joint variables of the hip and knee, which enables a robot to move the leg to the desired position through setting the required joint angles. However, a forward kinematic model does not support measuring the torque and forces on the joints to limit the range of motion.

Cadaver experiments in this study is a limited sample of 60-70-year-old males. To fully quantify the effect of other physiological factors (e.g. age, sex, etc.) on measurement uncertainty, a wide-range of cadavers are needed.

Since Grood and Suntay developed the knee JCS model [21], researches has shown it to be accurate [10]. Thus the knee translational error was not shown in real-time in this study; however, a point at 86^o of flexion was used to verify the foot positional error.

Measuring the knee translations in real-time is an open problem, and for this study were not measured or inferred during the experiments.

B. APPLICATIONS

The presented DH Parameter model of the human leg was specifically developed for automated leg manipulation during orthopaedic surgery. However, it can be used for applications ranging from robust human-robot designs to post-surgery rehabilitation.

The model will support leg manipulation without drilling supports for optical markers into a patient's leg as the current practice for replacement surgeries. For procedures where surgeons manually set the leg pose (such as a knee arthroscopy) without any information on the actual joint angles or joint gap size as shown in Figure 1b, the model can provide valuable insight to limit joint damage.

C. FUTURE WORK

Future work on a robot to manipulate the patient's foot will use the forward kinematic model of the leg developed in this study as input to an inverse 6DOF kinematic model of the robot manipulator, to automatically set the correct leg configuration for surgery. To support the use of the DH Parameter model and the error analysis in this study, it will be beneficial in future work to develop different models as a comparison.

For control and real-time measurement of the forces exerted on the joints, the current model can be extended to mitigate these forces. An inverse kinematic model needs to be developed from the model presented in this study to measure force and torque in each joint.

The foot model to the ground-truth difference in Figure 12 does not take into account the natural translation inside the knee joint. As seen from Table 1, it can be up to 21mm, if a surgeon or robotic manipulator exert forces on the knee joint. To accurately characterise the total foot positional error, the knee translations can be measured in real-time by using technologies such as Fluoroscopy.

The uncertainty in the foot position determines the precision that the hip and knee joints can be positioned during surgery. For instance, for knee arthroscopy, the instrument gap determines the damage caused during the surgery. With the complexity of the knee joint and the range of surgical position, it will be essential to determine how the uncertainty in the foot position influenced the internal knee structures.

Work is necessary to better characterise the measurement errors compared to the age and gender of candidates.

The presented methodology also carries the potential to be merged with the current state-of-the-art in arthroscopic SLAM [46] and introduce the robotic leg manipulation combined with visual navigation.

VI. CONCLUSION

A hip and knee robot model of the human leg was developed to present a nine degree of freedom system from which the standard DH parameters were defined. It forms the basis for automated control of a robotic leg manipulator, where traditionally surgeons manually manipulate a patient's foot to set the gap in the knee joint to allow surgical instruments.

During cadaver experiments, the leg was moved, and the positional data of the knee and foot recorded using an optical system. The hip and knee angles were calculated and used as input into the robot model, and the positional output of the model compared to that of the optically measure data. The measured knee positional error is 0.43mm, and when including the knee joint, it results in a maximum foot error of 3.51mm. It demonstrates that the robot model is highly suitable for leg manipulation during orthopaedic surgery.

ACKNOWLEDGMENT

The authors would like to thank Andres Marmol-Velez for his assistance during cadaver tests and Reuben Strydom for technology discussions reviewing this study.

Cadaveric experiments were approved by the Australian National Health and Medical Research Council (NHMRC)–Committee no. EC00171, Approval no. 1400000856.

REFERENCES

[1] J. J. Rice, "Healthcare bluebook," Healthcare Bluebook, Nashville, TN, USA, Tech. Rep. 2015, 2015. [Online]. Available: http://www.healthcarebluebook.com

[2] A. Jaiprakash, J. M. Roberts, and R. Crawford, "Perceptions of orthopaedic surgeons on knee arthroscopic surgery," *J. Orthopaedic Surg.*, 2016.

[3] M. Strydom, A. Jaiprakash, R. Crawford, T. Peynot, and J. M. Roberts, "Towards robotic arthroscopy: 'Instrument gap' segmentation," in *Proc. Australas. Conf. Robot. Autom.*, 2016, pp. 1–11.

[4] M. Strydom, R. Crawford, J. Roberts, and A. Jaiprakash, "Robotic arthroscopy: The uncertainty in internal knee joint measurement," *IEEE Access*, vol. 7, pp. 168382–168394, 2019.

[5] R. J. de Asla, L. Wan, H. E. Rubash, and G. Li, "Six DOF *in vivo* kinematics of the ankle joint complex: Application of a combined dual-orthogonal fluoroscopic and magnetic resonance imaging technique," *J. Orthopaedic Res.*, vol. 24, no. 5, pp. 1019–1027, Apr. 2006.

[6] T. R. Jenkyn and A. C. Nicol, "A multi-segment kinematic model of the foot with a novel definition of forefoot motion for use in clinical gait analysis during walking," *J. Biomech.*, vol. 40, no. 14, pp. 3271–3278, Jan. 2007.

[7] J. A. Reinbolt, J. F. Schutte, B. J. Fregly, B. I. Koh, R. T. Haftka, A. D. George, and K. H. Mitchell, "Determination of patient-specific multi-joint kinematic models through two-level optimization," *J. Biomech.*, vol. 38, no. 3, pp. 621–626, Mar. 2005.

[8] L. Blankevoort, R. Huiskes, and A. de Lange, "The envelope of passive knee joint motion," *J. Biomech.*, vol. 21, no. 9, pp. 705–720, Jan. 1988.

[9] P. Corke, *Robotics, Vision and Control: Fundamental Algorithms in MATLAB*, vol. 73. Berlin, Germany: Springer, 2011.

[10] H. Fujie, G. A. Livesay, M. Fujita, and S. L.-Y. Woo, "Forces and moments in six-DOF at the human knee joint: Mathematical description for control," *J. Biomech.*, vol. 29, no. 12, pp. 1577–1585, Dec. 1996.

[11] S. Głowiński and T. Krzyński, "An inverse kinematic algorithm for the human leg," *J. Theor. Appl. Mech.*, vol. 54, no. 1, pp. 53–61, 2016.

[12] K. Kaneko, K. Harada, F. Kanehiro, G. Miyamori, and K. Akachi, "Humanoid robot HRP-3," in *Proc. IEEE/RSJ Int. Conf. Intell. Robots Syst.*, Sep. 2008, pp. 2471–2478.

[13] B. M. Nigg and W. Herzog, *Biomechanics of the Musculo-Skeletal System*. Chichester, U.K.: Wiley, 1996.

[14] M. A. Ali, H. A. Park, and C. S. G. Lee, "Closed-form inverse kinematic joint solution for humanoid robots," in *Proc. IEEE/RSJ Int. Conf. Intell. Robots Syst.*, Oct. 2010, pp. 704–709.

[15] V. Joukov, M. Karg, and D. Kulic, "Online tracking of the lower body joint angles using IMUs for gait rehabilitation," in *Proc. 36th Annu. Int. Conf. IEEE Eng. Med. Biol. Soc.*, Aug. 2014, pp. 2310–2313.

[16] G. R. Scuderi and A. J. Tria, *The Knee: A Comprehensive Review*. Singapore: World Scientific, 2010.

[17] H. Bruyninckx, S. Demey, S. Dutré, and J. De Schutter, "Kinematic models for model-based compliant motion in the presence of uncertainty," *Int. J. Robot. Res.*, vol. 14, no. 5, pp. 465–482, Oct. 1995.

[18] M. Roche, "Robotic-assisted unicompartmental knee arthroplasty: The mako experience," *Clinics sports Med.*, vol. 33, no. 1, pp. 123–132, 2014.

[19] M. Strydom, A. Banach, L. Wu, A. Jaiprakash, R. Crawford, and J. Roberts, "Anatomical joint measurement with application to medical robotics," *IEEE Access*, vol. 8, pp. 118510–118524, 2020.

[20] R. S. Hartenberg and J. Denavit, "A kinematic notation for lower pair mechanisms based on matrices," *J. Appl. Mech.*, vol. 77, no. 2, pp. 215–221, 1955.

[21] E. S. Grood and W. J. Suntay, "A joint coordinate system for the clinical description of three-dimensional motions: application to the knee," *J. Biomech. Eng.*, 1983.

[22] G. R. Pennock and K. J. Clark, "An anatomy-based coordinate system for the description of the kinematic displacements in the human knee," *J. Biomech.*, vol. 23, no. 12, pp. 1209–1218, Jan. 1990.

[23] M. A. Lafortune, "The use of intra-cortical pins to measure the motion of the knee joint during walking," Ph.D. dissertation, Dept. Human Develop. Perform., PA State Univ., State College, PA, USA, 1984.

[24] J. H. Oliver and L. P. Coughlin, "Objective knee evaluation using the genucom knee analysis system: Clinical implications," *Amer. J. Sports Med.*, vol. 15, no. 6, pp. 571–578, Nov. 1987.

[25] F. C. Park, "Computational aspects of the product-of-exponentials formula for robot kinematics," *IEEE Trans. Autom. Control*, vol. 39, no. 3, pp. 643–647, Mar. 1994.

[26] L. Wu, R. Crawford, and J. Roberts, "An analytic approach to converting POE parameters into D–H parameters for serial-link robots," *IEEE Robot. Autom. Lett.*, vol. 2, no. 4, pp. 2174–2179, Oct. 2017.

[27] C.-C. Tsai, C.-C. Hung, and C.-F. Chang, "Trajectory planning and control of a 7-DOF robotic manipulator," in *Proc. Int. Conf. Adv. Robot. Intell. Syst. (ARIS)*, Jun. 2014, pp. 78–84.

[28] A. Williams and M. Logan, "Understanding tibio-femoral motion," *Knee*, vol. 11, no. 2, pp. 81–88, Apr. 2004.

[29] K. E. Moglo and A. Shirazi-Adl, "Cruciate coupling and screw-home mechanism in passive knee joint during extension–flexion," *J. Biomech.*, vol. 38, no. 5, pp. 1075–1083, May 2005.

[30] P. F. Hill, V. Vedi, A. Williams, H. Iwaki, V. Pinskerova, and M. A. Freeman, "Tibiofemoral movement 2: The loaded and unloaded living knee studied by MRI," *J. Bone Joint Surg. Brit. Volume*, vol. 82, no. 8, pp. 1196–1198, 2000.

[31] H. Iwaki, V. Pinskerova, and M. A. Freeman, "Tibiofemoral movement 1: The shapes and relative movements of the femur and tibia in the unloaded cadaver knee," *J. Bone Joint Surg. Brit. Volume*, vol. 82, no. 8, pp. 1189–1195, 2000.

[32] P. Johal, A. Williams, P. Wragg, D. Hunt, and W. Gedroyc, "Tibio-femoral movement in the living knee. A study of weight bearing and non-weight bearing knee kinematics using 'interventional' MRI," *J. Biomech.*, vol. 38, no. 2, pp. 269–276, Feb. 2005.

[33] M. A. R. Freeman and V. Pinskerova, "The movement of the normal tibio-femoral joint," *J. Biomech.*, vol. 38, no. 2, pp. 197–208, Feb. 2005.

[34] A. McPherson, J. Kärrholm, V. Pinskerova, A. Sosna, and S. Martelli, "Imaging knee position using MRI, RSA/CT and 3D digitisation," *J. Biomech.*, vol. 38, no. 2, pp. 263–268, 2005.

[35] A. Leardini, J. J. O'Connor, F. Catani, and S. Giannini, "A geometric model of the human ankle joint," *J. Biomech.*, vol. 32, no. 6, pp. 585–591, Jun. 1999.
[36] D. R. Wilson, J. D. Feikes, A. B. Zavatsky, and J. J. O'Connor, "The components of passive knee movement are coupled to flexion angle," *J. Biomech.*, vol. 33, no. 4, pp. 465–473, Apr. 2000.
[37] B. P. McKeon, J. V. Bono, and J. C. Richmond, *Knee Arthroscopy* (Number Book, Whole). New York, NY, USA: Springer, 2009.
[38] J. Apkarian, S. Naumann, and B. Cairns, "A three-dimensional kinematic and dynamic model of the lower limb," *J. Biomech.*, vol. 22, no. 2, pp. 143–155, Jan. 1989.
[39] S. Nussbaumer, M. Leunig, J. F. Glatthorn, S. Stauffacher, H. Gerber, and N. A. Maffiuletti, "Validity and test-retest reliability of manual goniometers for measuring passive hip range of motion in femoroacetabular impingement patients," *BMC Musculoskeletal Disorders*, vol. 11, no. 1, p. 194, 2010.
[40] P. Kouyoumdjian, R. Coulomb, T. Sanchez, and G. Asencio, "Clinical evaluation of hip joint rotation range of motion in adults," *Orthopaedics Traumatol., Surg. Res.*, vol. 98, no. 1, pp. 17–23, Feb. 2012.
[41] H. Prather, M. Harris-Hayes, D. M. Hunt, K. Steger-May, V. Mathew, and J. C. Clohisy, "Reliability and agreement of hip range of motion and provocative physical examination tests in asymptomatic volunteers," *PM&R*, vol. 2, no. 10, pp. 888–895, Oct. 2010.
[42] G. Li, M. Kozanek, A. Hosseini, F. Liu, S. K. Van De Velde, and H. E. Rubash, "New fluoroscopic imaging technique for investigation of 6DOF knee kinematics during treadmill gait," *J. Orthopaedic Surg. Res.*, vol. 4, no. 1, p. 6, Dec. 2009.
[43] M. F. Robinette and R. Manseur, "Robot-draw, an Internet-based visualization tool for robotics education," *IEEE Trans. Educ.*, vol. 44, no. 1, pp. 29–34, Feb. 2001.
[44] R. N. Jazar, *Theory of Applied Robotics: Kinematics, Dynamics, and Control*. New York, NY, USA: Springer, 2010.
[45] J. S. Dai, "Euler–Rodrigues formula variations, quaternion conjugation and intrinsic connections," *Mechanism Mach. Theory*, vol. 92, pp. 144–152, Oct. 2015.
[46] A. Marmol, A. Banach, and T. Peynot, "Dense-ArthroSLAM: Dense intra-articular 3-D reconstruction with robust localization prior for arthroscopy," *IEEE Robot. Autom. Lett.*, vol. 4, no. 2, pp. 918–925, Apr. 2019.

MARIO LLEWELLYN STRYDOM received the bachelor's degree in electronics and the master's degree in business. He is currently a Robotic Engineer and higher degree research candidate at the Australian Centre for Robotic Vision and the Queensland University of Technology. His research interests include computer vision and robot kinematics applied for medical robotics. He has published in the research areas of image segmentation, monocular joint measurement, and uncertainty, and has an approved patent for a robotic leg manipulator from the Australian patent office. He has 25 years of industry experience in the field of automation, electronics engineering, and information technology.

ARTUR BANACH received the Bachelor of Engineering degree in automatic control and robotics from the Poznan University of Technology, Poland, in 2016, and the Master of Research degree in medical robotics and image guided intervention from the Hamlyn Centre, Imperial College London, in 2017, where he introduced active constraints for tool-shaft collision avoidance in minimally invasive surgery on the Da Vinci Surgical System. He is currently pursuing the Ph.D. degree in surgical robotics with the Queensland University of Technology. His research interest includes innovating the field of surgery by looking for solutions to sublimely reduce patient suffering and improve quality of life.

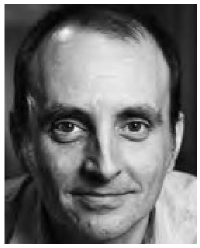

JONATHAN ROBERTS (Senior Member, IEEE) received the Ph.D. degree. He is currently a Professor in robotics with the Queensland University of Technology (QUT) and the Principal Supervisor for this research. After many years of industry experience in robotics, he is also leading medical robotics at QUT. He has held senior positions at CSIRO. He was the President of the Australian Robotics and Automation Association from 2007 to 2008. He is a member of the IEEE Robotics and Automation Society.

ROSS CRAWFORD received the Ph.D. degree from Oxford University. He is currently a Professor of orthopaedic research with QUT and undertakes private clinical practice at the Prince Charles and Holy Spirit Hospitals. He has mentored over 30 Ph.D. and M.Phil. students to the completion of their degrees and has a wealth of experience in teaching and leading researchers at all levels. He is currently a member of numerous medical committees. He has published more than 200 articles. As an Expert Surgeon, he assists with cadaver surgery experiments at the QUT Medical and Engineering Research Facility at the Prince Charles campus and brings significant knowledge of knee arthroscopy and the use of medical robotics to this research.

ANJALI TUMKUR JAIPRAKASH received the Med.Sc. degree. She is currently a Life Sciences Scientist and an Advance QLD Research Fellow of medical robotics with the Australian Centre for Robotic Vision and the Queensland University of Technology. She works at the intersection of medicine, engineering, and design developing medical devices for diagnosis and surgery, including the patented light field retinal diagnostic systems and vision-based robotic leg manipulation systems. She has experience in the field of orthopaedic research, optics, and design. She has extensive research experience in the hospital and clinical setting and the ethical conduct of research in compliance with the Australian Code for the Responsible Conduct of Research.